Comparative study on tensile and morphological properties of resin and rice husk reinforced polymer composite gyroid lattice structures

CHOUHAN, Ganesh, BIDARE, Prveen and MURALI, Gunji Bala

Comparative Study on Tensile and Morphological Properties of Resin and Rice Husk Reinforced Polymer Composite Gyroid Lattice Structures

Ganesh Chouhan[1*], Prveen Bidare[2], Gunji Bala Murali[3]

[1,3]School of Mechanical Engineering, Vellore Institute of Technology, Vellore, 632014, Tamil Nadu, India.
[2]Department of Engineering and Mathematics, College of Business, Technology and Engineering, Sheffield Hallam University, Sheffield S1 1WB, UK

Corresponding Author: ganesh.chouhan2020@vitstudent.ac.in

Abstract

This study aims to compare the tensile behaviour of 3d printed resin and rice husk-reinforced resin-based gyroid lattice structures. The work was completed in two phases, firstly a resin gyroid lattice structure with two design configurations of unit cell sizes (3, 4, 5, and 6) and solidity percentages (30, 40, and 50) was developed according to the ASTM638 (4) standard. The 12 designs were manufactured using VAT polymerization additive manufacturing and investigated for tensile strength. In the second phase, the poorest tensile testing results were chosen to develop the rice husk-reinforced resin samples with a mixing proportion of 10-20-30%. The experiment results revealed that the fracture is localized inside the gauge length according to the standard. Remarkably, the rice husk composite-based gyroid lattice samples exhibit 4.29, 6.55, and 9.35 times higher tensile strength than the selected resin sample (U_{3-30}). Additionally, a homogeneous distribution of rice husk particles has been observed in the micrograph analysis (SEM).

Keywords: Additive manufacturing, Gyroid, Lattice structure, Rice husk, Tensile strength

1. Introduction

Modern product development places significant emphasis on lightweight and durable design, which has become popular in many sectors such as aviation, automobiles, and healthcare. The adaptability of porous designs such as TPMS-based gyroid lattices has attracted considerable attention in recent years [1–4]. The numerous features include a higher surface area-to-volume ratio, lighting of the parts, a strongly ordered interconnected pore network, a self-supportive nature, and zero mean curvature help to achieve the desired performance in heat transfer devices, and structural parts [5]. However, it is quite challenging to manufacture such designs using traditional manufacturing methods [6].

Scientist Alan Schoen of NASA discovered the gyroid in 1970 [7]. They observed that it was a unique embedded section of the Schwarz P and D surface, with an approximate angle of association of 38.01. The gyroid is shown to be the only non-trivial member of the linked set. In addition to its distinctive features, there are parallel surface symmetry planes and a lack of right-angle sections on the surface. The existence of gyroid lattice has been documented by numerous scientists in a variety of natural objects, such as the retina of the human eye, butterfly plumage, blue morpho butterflies, emerald-patched cattle heart butterflies, and blue-winged leafbirds (see Figure **1**) [8]. In response to its better strength-to-volume ratio, the gyroid has already demonstrated its superior performance in a variety of areas, including aircraft wings [9], scaffolds for bone implants [10, 11], microreactors [12], and infill structures for mechanical tests [13].

The fourth industrial revolution, additive manufacturing (AM), provides designers with a significant deal of creative freedom while producing intricate, customized products. The most popular type of 3D printing is stereolithography (SLA), which can be used to print a variety of thermosetting materials owing to its ease of use and accessibility. Composite material development is a major industrial challenge, and many researchers are working to develop low-cost multi-material stereolithography 3D printers [14]. A wide range of organic materials, such as rice husk, wheat straw [15], wood [16], cork [17], and coconut coir, have been reinforced in resin to 3D print and successfully improved the mechanical properties.

Rice husk (RH) has been observed to be the most efficient low-cost organic material substitute for enhancing the mechanical properties of composite products. The major agricultural waste from rice production is rice husk, which is the result of rice milling. The disposal or recycling of rice waste has an impact on the economy and environment because it is not fully commercial for product-making. The chemical composition of rice husk consists

of silica (17–20%), cellulose (26–40%), and lignin (15–25%) [18]. Mehdi Shiva et al. [19] employed thermal and chemical methods to extract silica from rice husk for rubber formulations, whereas Kohei Morimoto et al. [20] discussed the useful applications of rice husk including, cement/concrete, adsorbents, soil conditioners, fertilizers, fibre-reinforced polymer composites, and metal matrix. Rice husk bonded with epoxy resin has improved mechanical properties through the use of varying mixing proportions (10-20-30 wt%) and developed via casting techniques [21]. The combination of rice husk and recycled polypropylene has been utilized to create effective 3D printing filaments. The rice husk weight ratio and raster angles are the key parameters of manufacturing [22]. Scientists are focusing on composite structures for better mechanical responses, including metal-plastic auxetic for predicting critical buckling stress [23], carbon nanotubes for enhancement in ballistic performance [24], and shape memory polymer composite for biomedical applications [25].

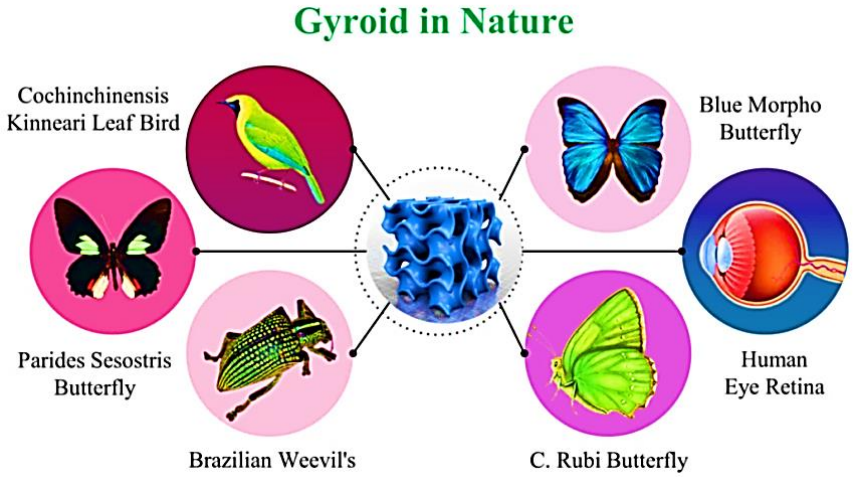

Figure 1 Sources of gyroid lattice in nature [8].

However, there is currently no research on the development of gyroid lattice structures made of rice husk composites that focus largely on mixing parameters with different materials. However, research on the use of rice husks to create lattice designs is lacking. This study examined the relationship between the solidity, unit cell size, mechanical properties, and material combination ratios.

This article presents an experimental and morphological comparison of resin and rice husk-reinforced resin-based gyroid lattice structures inspired by nature. The SLA 3D printing technique was used to develop the samples, which were intended to have four distinct unit cells and three solidity percentages. The tensile characteristics were examined concerning

unit cell sizes, mixing proportions, and solidity percentages. Furthermore, the distribution pattern of rice husk in 3d printed tensile samples has been addressed.

2. Materials and Methods

This section discusses the design and additive manufacturing of resin and rice husk-reinforced resin-based gyroid samples. In addition, morphological analysis has been discussed to understand the distribution behaviour of rice husks in resin.

2.1. Modeling Parameters of Gyroid Test Specimens

In the present study, TPMS-based gyroid lattice structures were used to design and analyze the tensile behaviour of polymeric and rice husk composite structures. These structures incorporate three solidity percentages (30-40-50) and four unit cell lengths (U_3-U_4-U_5-U_6). Following the specifications illustrated in **Figure 2**, 12 gyroid lattice structures with identical dogbone-like geometry have been created. The specimen was created utilizing ASTM D638 Type 4 samples standards, which address the tensile characteristics of polymers and were chosen as a foundation to meet the testing requirement. nTopology modeling software has been employed to design the gyroid test samples and the following implicit expressions can be used to express surfaces;

$$F_G(x,y,z) = \sin(\lambda_x x)\cos(\lambda_y y) + \sin(\lambda_y y)\cos(\lambda_z z) + \cos(\lambda_x x)\sin(\lambda_z z) = t \quad (1)$$

$$\lambda_i = \frac{2\pi}{L_i} \quad (\text{with } i = x, y, z)$$

Where L_i denotes unit cell length and depending on the design domain, t regulates the offset from the level sets.

The gauge area of the specimen was made of a lattice structure, and the grip portion was constructed in bulk, as illustrated in **Figure 2**, to guarantee structural stability during the tensile test. For each specimen, the same gauge size (33*6*3.2mm) was utilized, and unit cell sizes of 3 mm, 4 mm, 5 mm, and 6 mm were used.

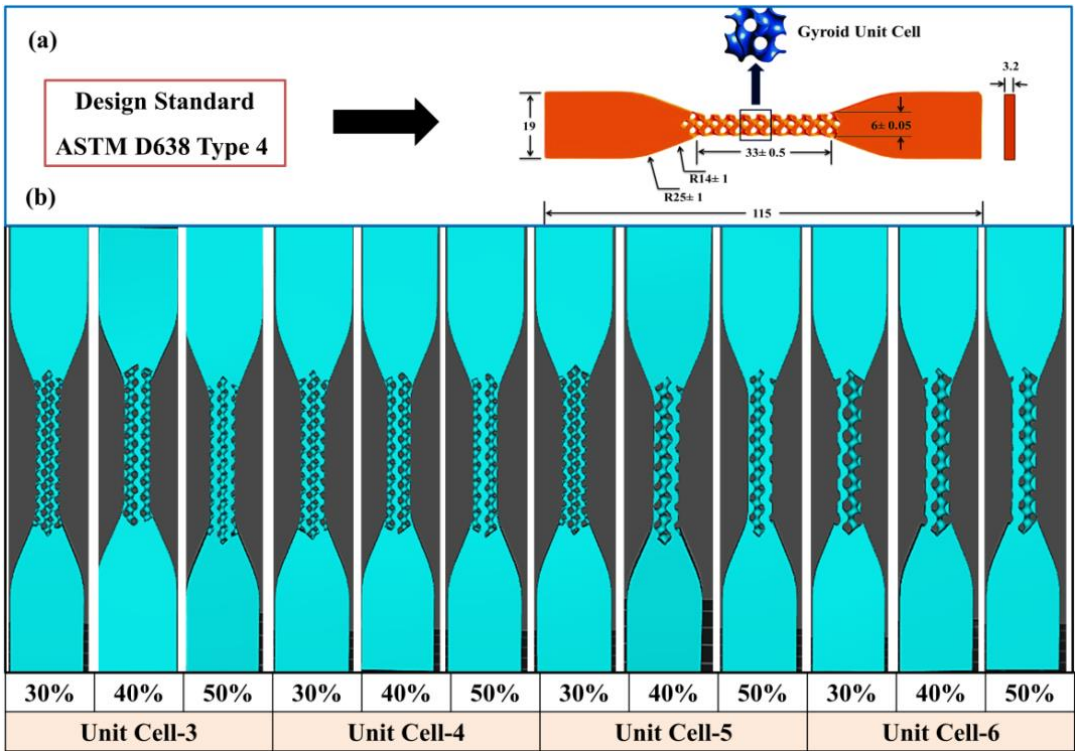

Figure 2 a) Tensile sample design according to ASTM D638 type 4 (unit-mm), and b) gyroid samples of different unit cell sizes (3,4,5,6) and solidity percentages (30-50%).

2.2. Sample Fabrication: (Resin gyroid samples)

This section describes the SLA 3D printing method utilized for generating the resin and rice husk mixed test sample. In recognition of the intricate nature of their design, gyroid lattices cannot be manufactured using conventional methods; however, their multiple advantages make them acceptable. Virtual models of the samples were saved in an STL file and imported into slicer software, which generates the digital layers. In order to conduct a comparative experimental investigation on the performance of gyroid lattice structures under tensile test, three samples have been additively manufactured for each unit cell design at a flat orientation.

The commercial SLA printer Creality LD002R LCD with a grey resin of ELEGOO ABS has been equipped with a 405 nm UV laser and a building speed of approximately 6-18 s/layer. Due to the extremely lightweight (approximately 8-10 grams) of the printed components, three samples were printed concurrently to conserve time. Additionally, the sample attempted to print at a build angle of 45 degrees, but the corner failed and a horizontal orientation was selected to conserve the material. The printing process for ABS-like resin is illustrated in **Figure 3**. The manufacturing process has been divided into two phases: twelve resin samples and nine rice husk-reinforced resin using a mixing ratio of 10-20-30%.

The level of accuracy of the prints is significantly influenced by the pre-processing phase in 3D printing, which encompasses everything from CAD files to machine settings. Preprocessing consists of inspecting the build plate for alignment, the build plate and tank for the absence of residue, and the condition of the FEP film that ensues to reduce the possibility of print failure. Furthermore, following the printing process, post-processing is crucial for transforming imperfect printed components into functional and visually appealing products. To eliminate any uncured resin, the gyroid-printed components underwent a 10-minute washing process with high-quality isopropyl alcohol. Subsequently, the cleansed samples were subjected to post-curing under UV light with a wavelength of 405 nm for 30 minutes. The structure becomes dense while increasing the size of unit cells and solidity percentage. The unit cell 3 and 30% solidity structure were very fragile and it was difficult to detach from the build platform.

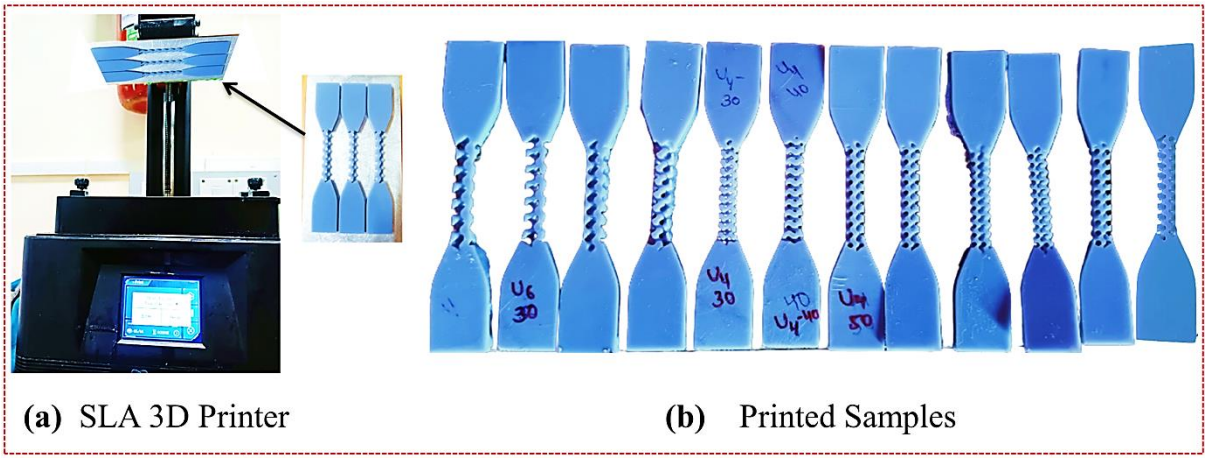

Figure 3 a) Stereolithography additive manufacturing process, and b) printed gyroid samples.

2.3. Fabrication of rice husk composites

The finely ground rice husk was procured from a nearby vendor and was free of dirt, dust, and other foreign matter on the fibre. It was allowed to absorb all surface moisture and become sufficiently dry through sun exposure for 10 hours; the particle size received was within the range of 0.212-0.850 mm, and a vibrating sieve system was used to achieve fine particle separation. Following that, the weight is assigned using the specified percentages (10, 20, 30g). A blend is made by combining 21 grams of rice husk powder with 210 grams of epoxy resin in a vessel (see Table 1). The reinforcement particles are now apparent since they are uniformly dispersed. In ten minutes of vigorous stirring in a stirring machine, and in order to properly combine the ingredients, the rice husk is gradually added while stirring and the solution turns into a viscous state.

A total of nine samples have been printed, three for each mixing ratio to check the distribution pattern, and almost identical patterns were noticed. During the printing, the process took two pauses, and the solution was stirred manually to avoid the bulk formation of husk powder. The process flow for the development of rice husk composite, from the raw husk to the final product, is shown in **Figure 4** and the distributional impact in samples is readily visible in these three samples (10-20-30%). The powder distribution difference in 10% and 30% samples can easily be visible with powder density. In all three structures, a smooth and balanced distribution of material has been noticed. Nonetheless, based on the mixing percentage the rice husk is visibly caught in the gyroid lattice outer curved surface, and maximum powder was found on 30% of samples. Table 2 demonstrates the chemical and physical properties of rice husks and resin.

Table 1 Experiment sequence concerning the amount of rice husk and epoxy resin.

Composition	Rice Husk	Epoxy Resin
10%	21g	210g
20%	42g	210g
30%	63g	210g

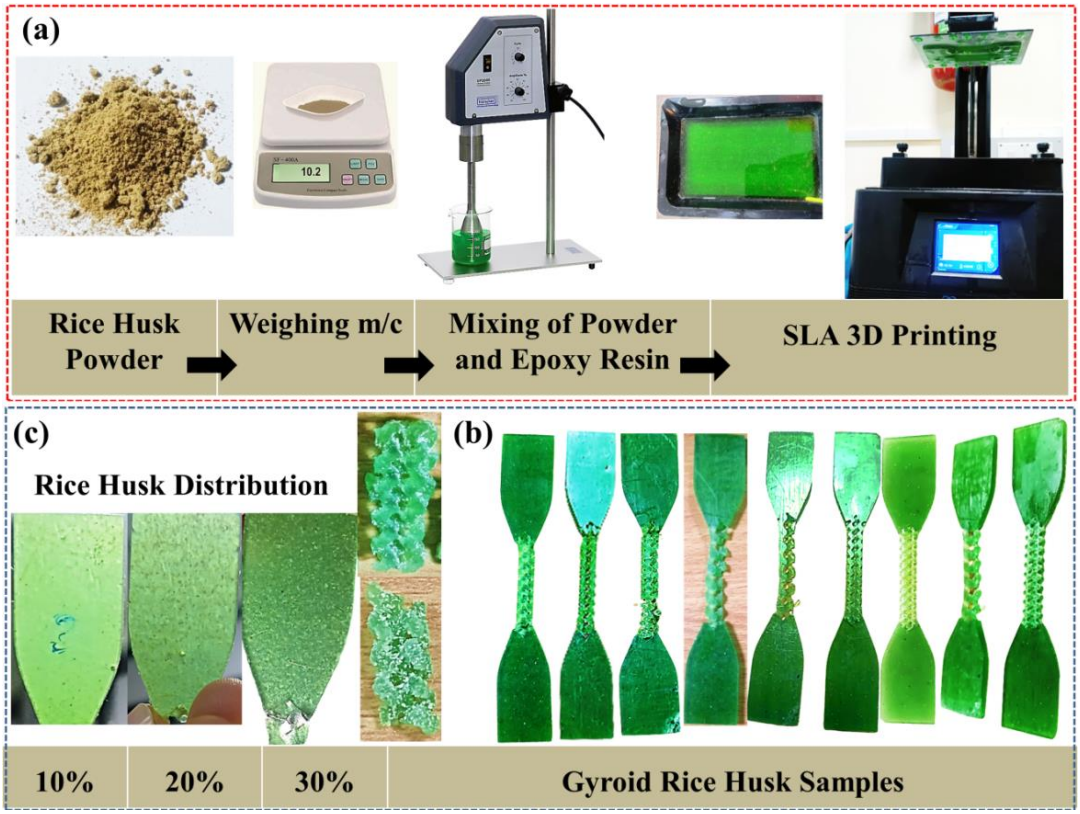

Figure 4 a) Development workflow of rice husk-based gyroid samples, b) digital image of printed samples, and c) rice distribution in samples according to mixing percentages and effects on the surface.

Table 2 Chemical composition and physical properties of rice husk and resin material [1, 26, 27].

Rice Husks		Resin	
Carbon	39.8-41.1	Polymer density (g/cm^3)	1.05-1.25
H	5.7-6.1	Tensile strength (MPa)	32-52
O	0.5-0.6	Modulus of elasticity (GPa)	1.0 - 2.65
N	37.4-36.6	Shrinkage (%)	3.72-4.24
Bulk density (kg/m^3)	90–150	Elongation at Break (%)	3.00 -150
Calorific value (KJ/kg)	15217.20	Melting temperature (^{0}C)	150-162

2.4. Mechanical Testing and Microstructure Analysis

As seen in **Figure 5**, the tensile test was performed on UTM using INSTRON 8801. The specimens were made following ASTM D638 specifications. The experiments were conducted with a temperature of 26 ºC and a relative humidity of 60%. For a specimen with a length of 115 mm, the measured span length was 33 mm. The lower plate was fixed for the tensile testing, and samples were positioned between the two plates. On the tensile plate, the lattices were oriented in the same manner as they had been printed. The machine was positioned in the centre of the span length, and the load was delivered progressively at a strain rate of 2 mm/min. Bluehill software was used to continuously assess the stress and strain. The testing procedure and deformed samples are displayed in **Figure 5**. The key observation is that a single lattice row is involved in every fracture, which occurs inside the gauge length. This indicates a steady load transfer throughout testing.

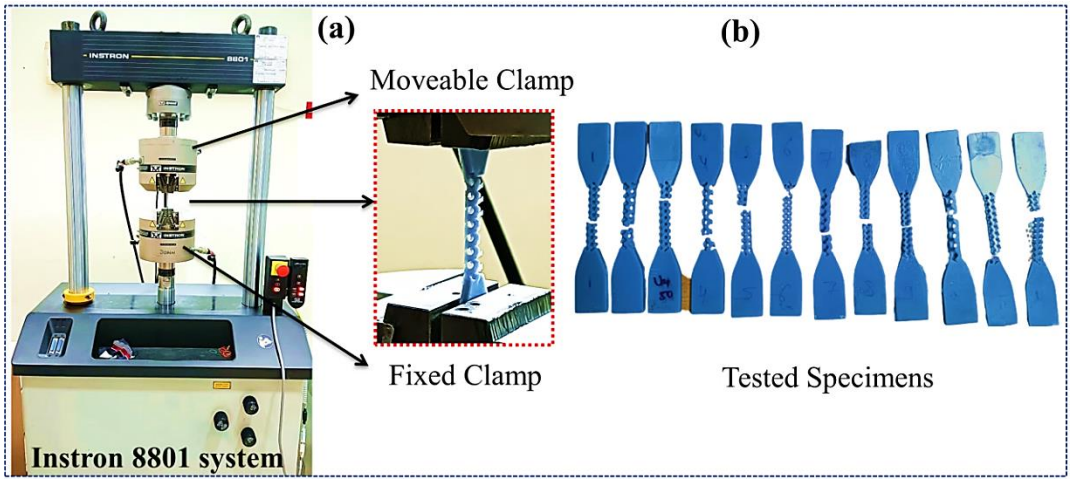

Figure 5 a) The schematic of tensile tests UTM setup, and b) the location of the fracture in tested samples.

The surface morphology of the rice husk composite gyroid samples was examined after the tensile test. The surface properties of the gyroid samples have been compared for different locations using field emission scanning electron microscopy (FESEM) research. The standard metallographic approach was followed to observe the microstructure of the sample. The test

samples were prepared with a size of 1×1 cm^2 and the fracture surface was coated with vanadium sputter before analysis on FEI Quanta 250 field emission gun (FEG). The primary aim of scanning is to study the rice husk distribution pattern in gyroid resin samples, fracture points, and void generation. The SEM images of the corresponding tensile tests (10-20-30%) samples are displayed in **Figure 6** and **Figure 7** which show the presence of the microstructure of rice husk in the mixture.

The images have been pointed for the grip area and gyroid unit cell at the gauge section. In all three mixing proportion structures, there were variations in both the quantity and size of husk particles. However, the uniaxial orientation of the husk particles in the 10% RH mixture is confirmed by the appearance of the particles as tiny strands and long cracks. There are little clumped areas in the 20% combination, but the 30% mixture includes much larger ones. In the test samples of the 10% and 20% RH mixture, the husk distribution is uniform, but in the 30%, it is irregular. Gyroid samples with 20% mixing contain microvoids. **Figure 7** illustrates that the gyroid unit cell has a uniform distribution of rise husk with tiny holes, and all three samples have a good flow of RH material.

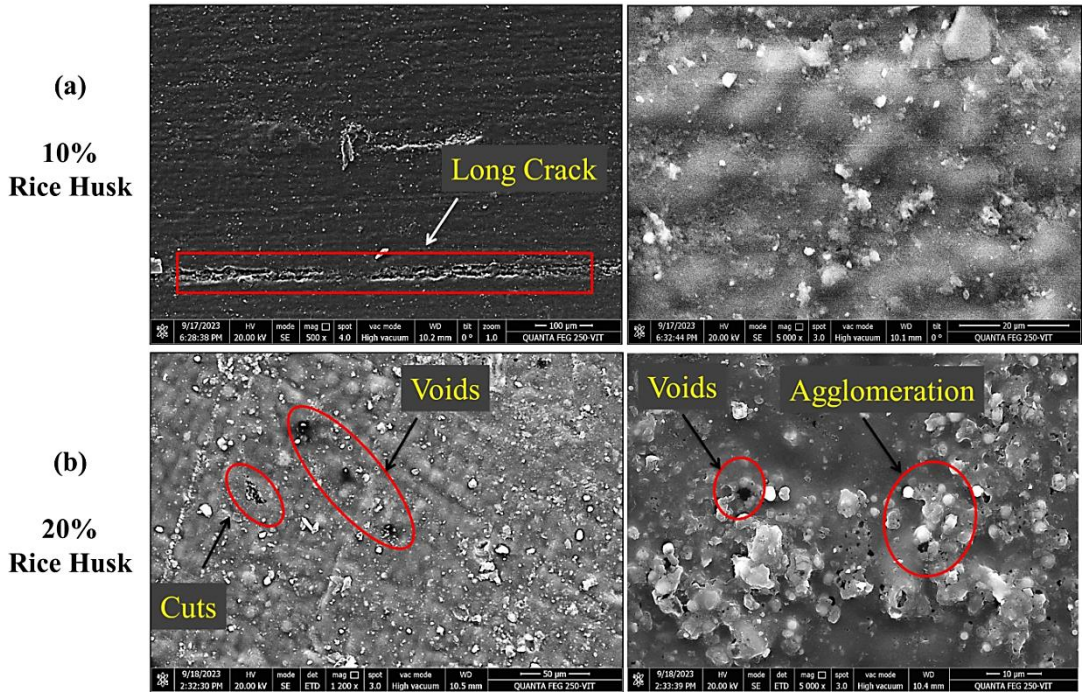

Figure 6 FESEM results for irregularities in a) 10% mixed RH, and b) 20% mixed RH composite gyroid lattice structure (Grip area).

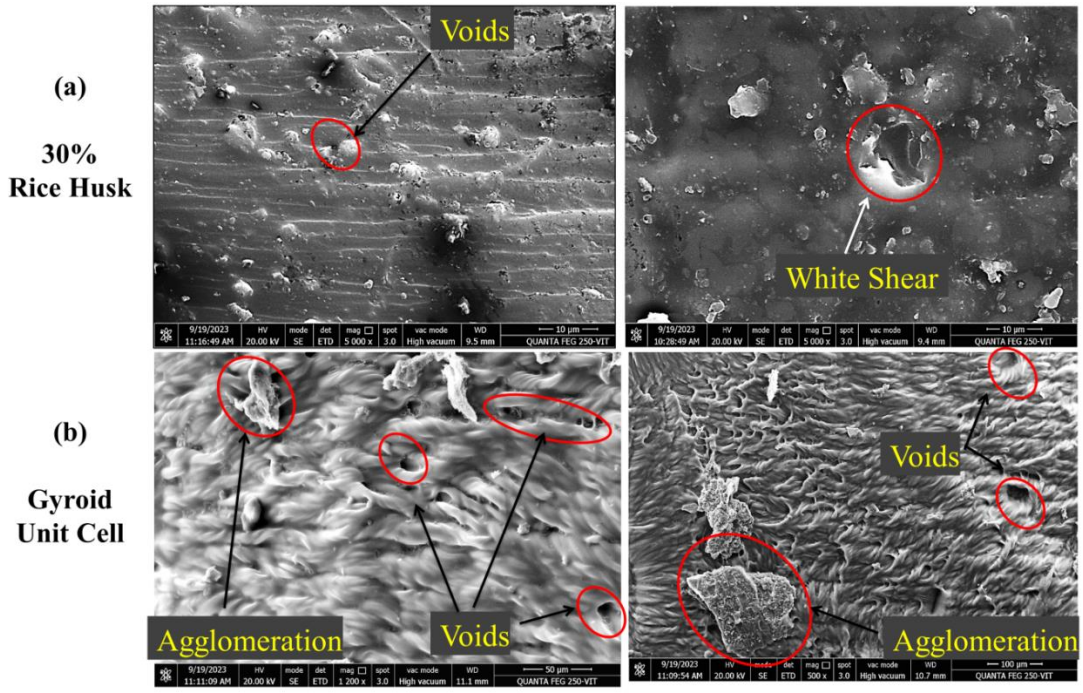

Figure 7 FESEM results for irregularities in a) 30% mixed RH gyroid (Grip area), and b) gyroid lattice unit cell.

3. Results and Discussion

The comparative study presents the results evaluated from multiple perspectives. The Mechanical properties have been influenced by the unit cell and solidity percentage under tensile stress. In addition, the print accuracy of 3D-printed pure resin and rice husk composite gyroid samples has been discussed.

3.1. Preliminary Results of Epoxy Resin Test

Figure 8 exhibits the stress-strain curves for the gyroid-based tensile samples, while Table 3 provides details about the cross-section and mechanical characteristics. The testing results for each gyroid lattice sample observed linear behaviour at the beginning and then brittle deformation with a higher stress of 9-12 MPa has been recorded. As a result, at various points for every specimen, this trend significantly changed as the ultimate strength (limited plastic region) was reached. A brittle fracture of the struts at very low strain was found in tensile loading at the end of the testing. The most important finding is that every fracture included a single lattice row and occurred inside the lattice section of the gauge length. This validates the introduction of a steady load during the testing. The complexity and topology of the gyroid lattice influenced the tensile strength and the extension of the plastic zone. As a point of fact, the lattice complexity results in an uneven distribution of stress throughout the cell. A little necking and brittle failure has been observed. The highest loading capacity for gyroid

lattice samples with solidities of 40% and 50% has been measured. According to a comparison of these results, the unit cell 3 gyroid structure proved to be the most appropriate structure for tensile stress ($U_{3\text{-}40}$-12 MPa, $U_{3\text{-}50}$-6 MPa) although all unit cell gyroid structures achieved nearly equal strength in the case of lower solidity. However, 50% solidity gyroid samples show better tensile strength.

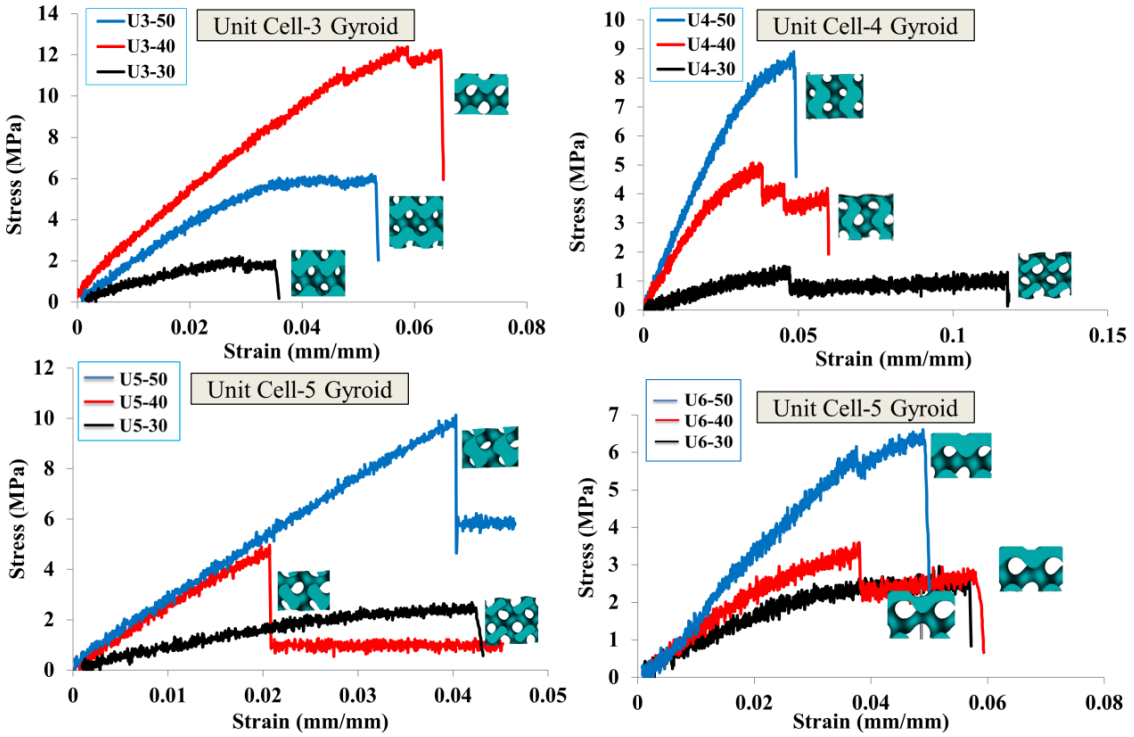

Figure 8 The impact of the various unit cell sizes (3,4,5,6) and solidity percentage (30-50%) of gyroid lattice structure on the tensile behaviour.

Table 3 The mechanical characteristics of the gyroid lattice structures.

Gyroid Sample	Maximum Load (N)	UTS (MPa)	Young's Modulus (MPa)	Elongation at Break (Standard) %
$U_{3\text{-}30}$	46.59	2	206.98	5.90
$U_{3\text{-}40}$	260.16	12	289.05	7.11
$U_{3\text{-}50}$	130.33	6	2086.98	4.16
$U_{4\text{-}30}$	31.87	2	952.71	12.23
$U_{4\text{-}40}$	106.53	5	208.73	7.34
$U_{4\text{-}50}$	186.96	9	262.30	5.17
$U_{5\text{-}30}$	58.56	2	255.20	5.23
$U_{5\text{-}40}$	103.68	5	294.86	4.52
$U_{5\text{-}50}$	211.89	10	267.25	4.65
$U_{6\text{-}30}$	62.19	3	92.63	6.05
$U_{6\text{-}40}$	75.53	4	119.16	6.01
$U_{6\text{-}50}$	138.80	7	204.57	7.53

3.2. Determination of print accuracy

The tensile test specimens were measured using a digital Vernier calliper. **Figure 9**a shows the accuracy average of the tensile test samples for width, and thickness. For every specimen,

the dimensions were checked at the gauge and grip area. The observed outcomes are presented in relation to the actual values (thickness "t" = 3.2 mm and width "b" = 6 mm). There was no noticeable difference seen in the tested samples' measurements. However, the gyroid curved surface caused a small reduction in specific conditions. Every specimen has excellent length precision, which is in good alignment with the actual number. The high-quality outer surface finish has been achieved via SLA 3D printing and no print lines are visible on the outer surface. In theory, good width results are anticipated for flat-oriented printed samples. The test findings, however, indicate a strong similarity between the Flat orientation printed samples. For samples with low solidity, the print accuracy averages 98.61%, whereas for samples with higher solidity, it averages 99.54%. As a result, the average processing accuracy across all tensile test specimens is 99.11%.

Figure 9b presents a broad overview of the influence of the structure type with all three solidities of tensile strength. The histograms demonstrate that the structures with higher solidity obtained the best overall tensile strength results, while the structures with lesser solidity performed the worst. Among all the structures, unit cell 3's structure with 40% solidity has the highest tensile strength (12 MPa). This is a result of the highest possible number of unit cells in a compact size and average solidity turning into a strong structure that is consistent with the direction of the tensile force, the best feature for handling unidirectional forces. In addition, the average tensile strength for structures with 30% solidity shows fairly close results in all unit cells. However, when the solidity increased the variation in tensile strength for the other unit cell structures (U_4-U_5-U_6) became more noticeable. This is because, in structures with small solidities, all struts are thin, and the gyroid structure's overall tensile performance is determined by its vertical struts. The strength of the three structures becomes closer as solidity rises because the struts go wider and the support between the vertical struts decreases significantly.

Figure 9c compares the elongation at break values of all unit cell gyroid configurations. It is evident that across the whole solidity range, relatively similar values and no discernible pattern have been observed. The tested gyroid lattice sample U4-30 had the maximum elongation at break (12.23%), whereas U5-40 sample had the lowest (4.52%). The stiffness of the finished product is largely determined by Young's modulus. Figure 9d demonstrates the tensile modulus of gyroid lattices.

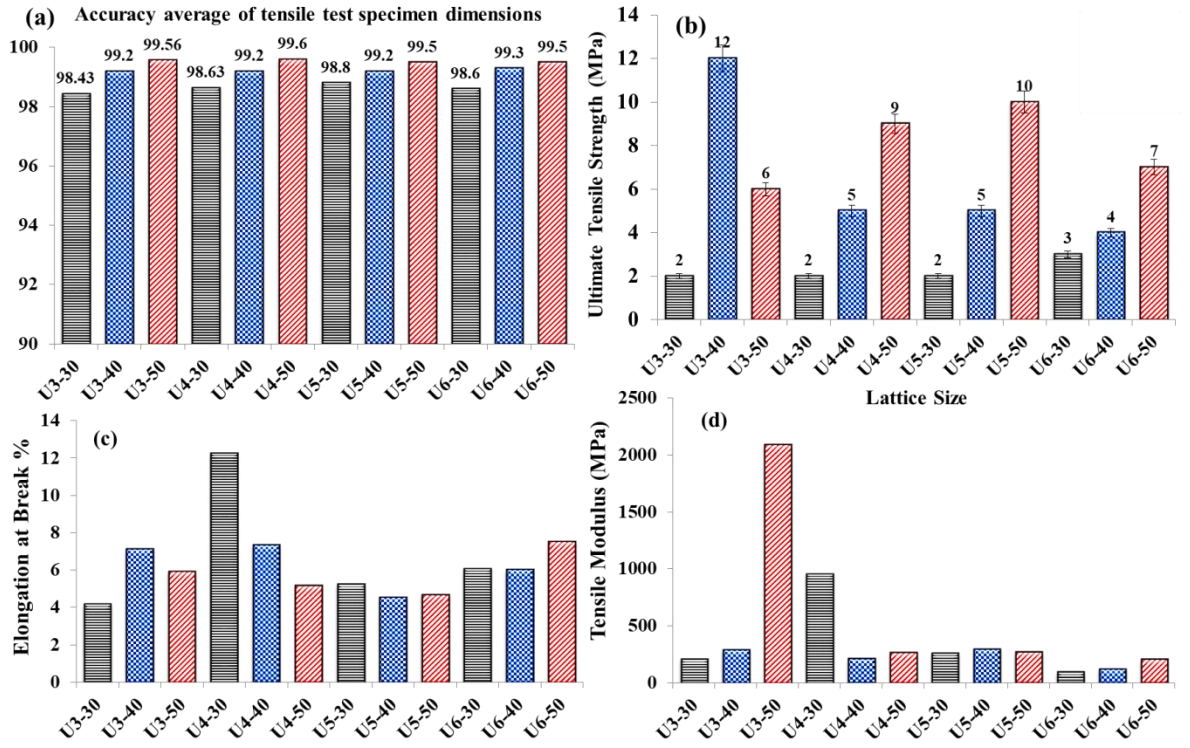

Figure 9 Testing performance of gyroid lattices, a) Printing accuracy of samples, and b-d) mechanical properties ultimate tensile strength, elongation percentage, and tensile modulus.

3.4. Comparison based on Rice husk composition

In the current work, unit cell 3 with 30% solidity was considered for the production of rice husk composite gyroid samples. The $U_{3\text{-}30}$ sample was chosen because of its unsatisfactory mechanical characteristics. Nine samples have been printed with mixing proportions of 10%, 20%, and 30% rice husk to compare and analyze the mechanical properties. The average values of tensile results have been selected for comparison for each mixing proportion. Tensile test results and extracted effects on mechanical properties from plots for rice husk composite samples are shown in **Figure 10**. For rice husk mixing at 10%, 20%, and 30%, the calculated highest tensile strengths were 8.56 MPa, 13.1 MPa, and 18.7 MPa; the corresponding Young moduli were 541 MPa, 485 MPa, and 718 MPa; and the corresponding tensile strain to break was 2.2%, 6.10%, and 6.22%. Compared to the pure resin sample $U_{3\text{-}30}$, these values are extremely high. It appears that the tensile strength of the composites increases with an increase in the percentage of rice husk. On the other hand, a 30% rice husk mixture demonstrated extraordinarily high tensile strength (18.7 MPa). Higher rice husk in the pure resin promotes stronger bonding, which ultimately results in a stronger boost to strength. The gauge areas of printed rice husk composite samples are less accurate than those of pure resin samples. The rice husk gyroid structure has recorded 4 times higher loading

capacity and improved strain performance than pure resin gyroid samples. Figure **10**b presents the stress-strain curve in which multiple yielding has been observed due to fracture of unit cells.

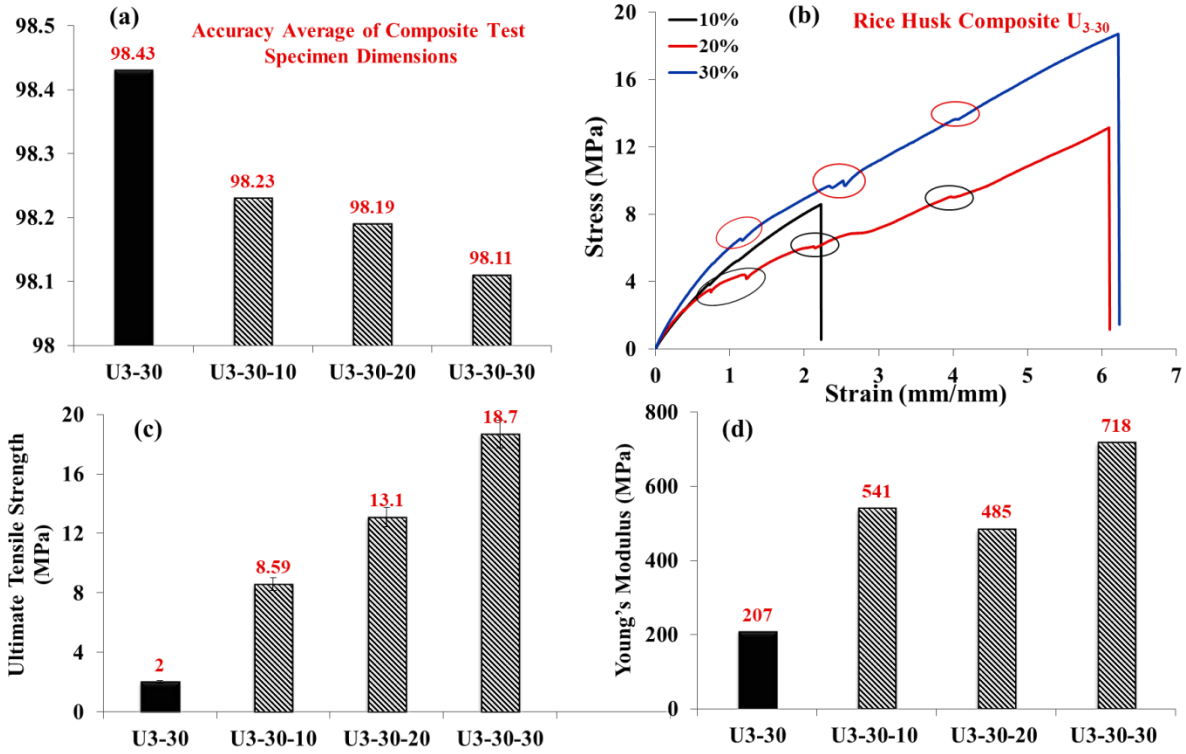

Figure 10 Impact of the type of rice husk mixing on (a) print accuracy, (b) stress-strain curves, (c) ultimate tensile strength, and (d) Young´s modulus; for all gyroid lattices.

4. Conclusion

In this work, a TPMS-based gyroid lattice structure with four distinct unit cell sizes and three solidity rates has been numerically designed and manufactured by SLA additive manufacturing for tensile testing. Two phases have been proposed for the work and primarily investigated the tensile strength of 12 resin gyroid samples. In the next phase, nine rice husk composite samples with mixing ratios of 10%, 20%, and 30% have been produced using the targeted design $U_{3\text{-}30}$. Additionally, to understand the distribution of powder, a morphological study has been presented. The investigation yielded the subsequent conclusions.

- The experimental results indicate that the 30% solidity resin gyroid structures in each unit cell category are the least appropriate for tensile stress from the perspective of ultimate stress. The 50% solidity gyroid samples in all unit cell ranges show higher tensile strength, compared to unit cell three is 3.5 times, unit cell four is 4.5 times, unit cell five is 5 times, and 2.5 times higher than unit cell six samples.

- The mixing proportion of 30% rice husk and 70% resin produced the most superior samples. The tensile strength was reported to be 9.35% higher than the resin sample.
- Overall mechanical characteristics were boosted by the combination of rice husk grains and resin material since the print accuracy decreased significantly.
- In all mixing proportions samples, the presence of rice husk in resin is evident.
- Following the tensile tests, FESEM examinations were performed, and the tested rice husk composite samples displayed uniform distribution, long cracks, micro-voids, and agglomeration.

This study provides a foundation for researchers in the future who may use the same materials (rice husk and resin) for different applications. This research will open up many new possibilities for future investigation of major lightweight and high-strength materials. However, the study still leaves an opportunity for the researchers to perform additional research in areas like:

- Performing Manufacturing and testing of high-strength samples (solidity 40 and 50% in all unit cell categories).
- To study small mixing ratios and their effect on tensile properties.
- Performing manufacturing and testing of the composite samples for compressive characteristics

Declarations

Conflicts of Interest: The authors declared no conflict of interest.

Acknowledgement: Not applicable.

Availability of data and materials

The data used for finding the results are been included in the manuscript.

Funding: No funding is associated with this research.

Ethical approval: The authors declare that there is no ethical issue applied to this article.

Abbreviations

SEM	Scanning electron microscopy
UTS	Universal testing machine
SLA	Stereolithography
TPMS	Triply periodic minimal surface
RH	Rice husk
CAD	Computer-aided design
ASTM	American Society for Testing and Materials
AM	Additive Manufacturing
UV	Ultraviolet

STL	Standard triangle language
FEP	Fluorinated Ethylene Propylene
UC	Unit cell
3D	Three dimensional

References

1. Chouhan G, Bala Murali G (2023) Uniform and graded bio-inspired gyroid lattice: Effects of post-curing and print orientation on mechanical property. Proc Inst Mech Eng Part L J Mater Des Appl 0: https://doi.org/10.1177/14644207231200729

2. Dixit T, Al-Hajri E, Paul MC, et al (2022) High performance, microarchitected, compact heat exchanger enabled by 3D printing. Appl Therm Eng 210:118339. https://doi.org/10.1016/J.APPLTHERMALENG.2022.118339

3. Caiazzo F, Alfieri V, Guillen DG, Fabbricatore A (2022) Metal functionally graded gyroids: additive manufacturing, mechanical properties, and simulation. Int J Adv Manuf Technol 123:2501–2518. https://doi.org/10.1007/s00170-022-10334-9

4. Timercan A, Sheremetyev V, Brailovski V (2021) Mechanical properties and fluid permeability of gyroid and diamond lattice structures for intervertebral devices: functional requirements and comparative analysis. Sci Technol Adv Mater 22:285–300

5. Samson S, Tran P, Marzocca P (2023) Design and modelling of porous gyroid heatsinks: Influences of cell size, porosity and material variation. Appl Therm Eng 235:121296. https://doi.org/10.1016/j.applthermaleng.2023.121296

6. Ramos H, Santiago R, Soe S, et al (2022) Response of gyroid lattice structures to impact loads. Int J Impact Eng 164:104202. https://doi.org/10.1016/J.IJIMPENG.2022.104202

7. Maharjan GK, Khan SZ, Riza SH, Masood SH (2018) Compressive Behaviour of 3D Printed Polymeric Gyroid Cellular Lattice Structure. IOP Conf Ser Mater Sci Eng 455:012047. https://doi.org/10.1088/1757-899X/455/1/012047

8. Chouhan G, Bala Murali G Designs, advancements, and applications of three-dimensional printed gyroid structures: A review. Proc Inst Mech Eng Part E J Process Mech Eng 2023;0(0). https://doi.org/10.1177/09544089231160030

9. Lobitz L, Traub H, Overbeck M, et al (2023) Aircraft Wing Design for Extended Hybrid Laminar Flow Control. aerospace 10:1–16

10. Oladapo BI, Kayode JF, Karagiannidis P, et al (2022) Polymeric composites of cubic-octahedron and gyroid lattice for biomimetic dental implants. Mater Chem Phys 289:126454. https://doi.org/10.1016/j.matchemphys.2022.126454

11. Ataee A, Li Y, Brandt M, Wen C (2018) Ultrahigh-strength titanium gyroid scaffolds manufactured by selective laser melting (SLM) for bone implant applications. Acta Mater 158:354–368. https://doi.org/10.1016/J.ACTAMAT.2018.08.005

12. Baena-Moreno FM, González-Castaño M, Navarro De Miguel JC, et al (2021) Stepping toward Efficient Microreactors for CO2Methanation: 3D-Printed Gyroid Geometry. ACS Sustain Chem Eng 9:8198–8206. https://doi.org/10.1021/ACSSUSCHEMENG.1C01980/ASSET/IMAGES/MEDIUM/SC1C01980_0009.GIF

13. Birosz MT, Ledenyák D, Andó M (2022) Effect of FDM infill patterns on mechanical properties. Polym Test 113:107654. https://doi.org/10.1016/j.polymertesting.2022.107654

14. Khatri B, Frey M, Raouf-Fahmy A, et al (2020) micromachines Development of a Multi-Material Stereolithography 3D Printing Device. Micromachines 11:. https://doi.org/10.3390/mi11050532

15. Romero-Ocaña I, Delgado NF, Molina SI (2022) Biomass waste from rice and wheat straw for developing composites by stereolithography additive manufacturing. Ind Crops Prod 189:115832. https://doi.org/10.1016/J.INDCROP.2022.115832

16. Zhang S, Bhagia S, Li M, et al Wood-reinforced composites by stereolithography with the stress whitening behavior. Mater Des 206:109773. https://doi.org/10.1016/j.matdes.2021.109773

17. Romero-Ocaña I, Molina SI (2022) Cork photocurable resin composite for stereolithography (SLA): Influence of cork particle size on mechanical and thermal properties. Addit Manuf 51:. https://doi.org/10.1016/j.addma.2021.102586

18. Dien LQ, Chung NH, Thi Van Anh N, et al (2022) Rice husk integrated biochemical refinery for the production of nano- and bioproducts. Process Biochem 121:647–655. https://doi.org/https://doi.org/10.1016/j.procbio.2022.08.009

19. Shiva M, Golmohammadi M, Nouroozi F (2023) Extraction of silica from rice husk for rubber-cord adhesion systems of tire industry. Biomass Convers Biorefinery.

https://doi.org/10.1007/s13399-023-03893-8

20. Morimoto K, Tsuda K, Mizuno D (2023) Literature Review on the Utilization of Rice Husks: Focus on Application of Materials for Digital Fabrication. Materials (Basel). 16

21. Jain N, Somvanshi KS, Gope PC, Singh VK (2019) Mechanical characterization and machining performance evaluation of rice husk/epoxy an agricultural waste based composite material. J Mech Behav Mater 28:29–38. https://doi.org/10.1515/jmbm-2019-0005

22. Morales MA, Atencio Martinez CL, Maranon A, et al (2021) Development and Characterization of Rice Husk and Recycled Polypropylene Composite Filaments for 3D Printing. Polymers (Basel). 13

23. Box F, Johnson CG, Pihler-Puzović D (2020) Hard auxetic metamaterials. Extrem Mech Lett 40:100980. https://doi.org/https://doi.org/10.1016/j.eml.2020.100980

24. Gibson J, McKee J, Freihofer G, et al (2014) International Journal of Smart and Nano Materials Enhancement in ballistic performance of composite hard armor through carbon nanotubes. Int J Smart Nano Mater 4:. https://doi.org/10.1080/19475411.2013.870938

25. Zhao W, Huang Z, Liu L, et al (2021) Porous bone tissue scaffold concept based on shape memory PLA/Fe3O4. Compos Sci Technol 203:108563. https://doi.org/https://doi.org/10.1016/j.compscitech.2020.108563

26. Korotkova TG, Ksandopulo SJ, Donenko AP, et al (2016) Physical properties and chemical composition of the rice husk and dust. Orient J Chem 32:3213–3219. https://doi.org/10.13005/ojc/320644

27. Babaso PN, Sharanagouda H (2017) Rice Husk and Its Applications: Review. Int J Curr Microbiol Appl Sci 6:1144–1156. https://doi.org/10.20546/ijcmas.2017.610.138